

A Modern View on the Red Sea Rift: Tectonics, Volcanism and Salt Blankets

Nico Augustin, Colin W. Devey, and Froukje M. van der Zwan

Abstract

Continental rifting and ocean basin formation can be observed at the present day in the Red Sea, which is used as the modern analogue for the formation of mid-ocean ridges. Competing theories for how spreading begins—either by quasi-instantaneous formation of a whole spreading segment or by initiation of spreading at multiple discrete “nodes” separated by thinned continental lithosphere—have been put forward based, until recently, on the observations that many seafloor features and geophysical anomalies (gravity, magnetics) along the axis of the Red Sea appeared anomalous compared to ancient and modern examples of ocean basins in other parts of the world. The latest research shows, however, that most of the differences between the Red Sea Rift (RSR) and other (ultra)slow-spreading mid-ocean ridges can be related to its relatively young age and the presence and movement of giant submarine salt flows that blanket large portions of the rift valley. In addition, the geophysical data that was previously used to support the presence of continental crust between the axial basins with outcropping oceanic crust (formerly named “spreading nodes”) can be equally well explained by processes related to the sedimentary blanketing and hydrothermal alteration. The observed spreading nodes are not separated from one another by tectonic boundaries but rather represent “windows” onto a continuous spreading axis which is locally inundated and masked by massive slumping of sediments or evaporites from the rift flanks. Volcanic and tectonic morphologies are comparable to those observed along slow and ultra-slow spreading ridges elsewhere and regional systematics of volcanic

occurrences are related to variations in volcanic activity and mantle heat flow. Melt-salt interaction due to salt flows, that locally cover the active spreading segments, and the absence of large detachment faults as a result of the nearby Afar plume are unique features of the RSR. The differences and anomalies seen in the Red Sea still may be applicable to all young oceanic rifts, associated with plumes and/or evaporites, which makes the Red Sea a unique but highly relevant type example for the initiation of slow rifting and seafloor spreading and one of the most interesting targets for future ocean research.

1 Introduction

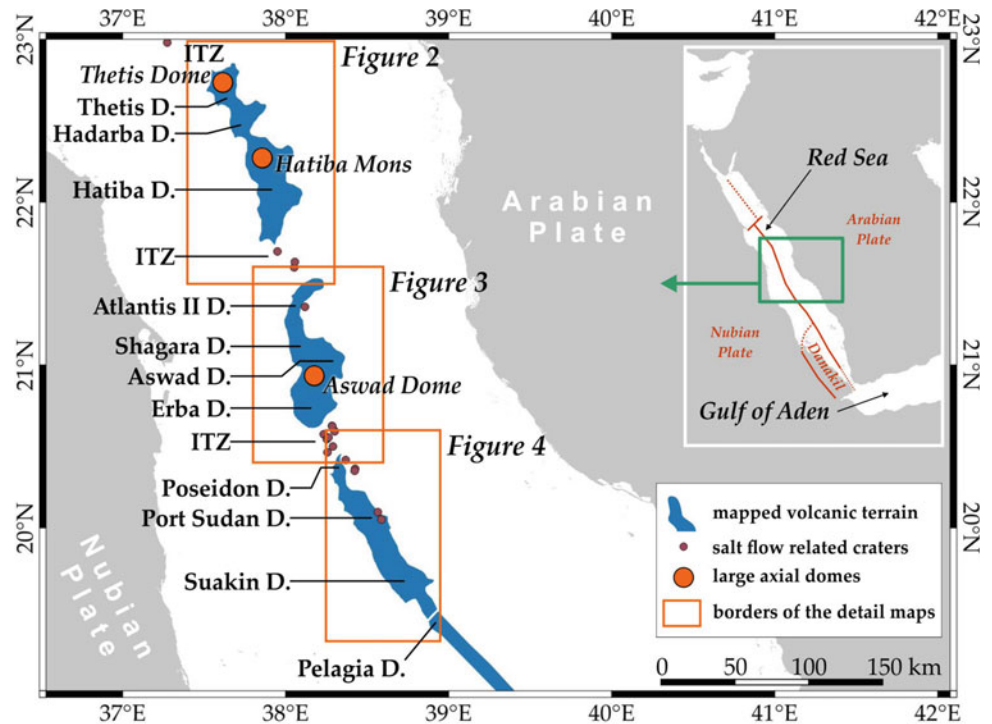
Plate tectonics has been splitting continents and opening new oceans for at least half of all Earth history (Kerrich and Polat 2006). But how the transition from rifting continental lithosphere to spreading new oceanic lithosphere (Courtilot 1982; Whitmarsh et al. 2001) occurs is unclear. Competing hypotheses suggest either geologically instantaneous establishment of a new spreading segment (e.g., Taylor et al. 1995) or the formation of discrete spreading “nodes” within the stretched continent whose activity may continue for several Ma before the continent is finally sundered (Bonatti 1985; Ligi et al. 2012).

Continental rifting and the transition to spreading can be observed at present in the Woodlark Basin (Taylor et al. 1995) and the Red Sea (Bonatti 1985). The point at which rifting changes to spreading in the Woodlark Basin is well defined and migrates westward into the continent by the abrupt initiation and rapid ($\approx 500 \text{ mm yr}^{-1}$) propagation of a new spreading segment within the rifted crust. The change from rifting to spreading in the Woodlark Basin occurs after a relatively constant $200 \pm 40 \text{ km}$ of overall stretching, consistent with observations from older passive margins such as the northern Atlantic margins, the Eurasian basin and its adjacent margins (e.g., Taylor et al. 1999; White and

N. Augustin (✉) · C. W. Devey · F. M. van der Zwan
GEOMAR Helmholtz Centre for Ocean Research Kiel,
Wischhofstraße 1-3, 24148 Kiel, Germany
e-mail: naugustin@geomar.de

F. M. van der Zwan
Institute of Geosciences, Christian Albrechts University Kiel,
Ludewig-Meyn-Straße 10, 24118 Kiel, Germany

Fig. 1 Overview of the study area with main geographic features, the mapped volcanic terrain (blue areas), large axial dome-shaped volcanoes (orange circles), salt flow related craters (dots) and the borders of the detailed maps shown in Figs. 2, 3, 4. The inset also shows the approximate positions of plate boundaries in the Red Sea (red lines). After Augustin et al. (2016) with permission of Elsevier



McKenzie 1989; Grachev 2003). During its rapid propagation, the new axis is separated from the adjacent previously established axis by an accommodation zone composed of rifting continental crust into which the new axis propagates. When propagation ceases, the new axis develops an overlap-type boundary to the adjacent segment, which can, with continued spreading, evolve into a transform fault (Taylor et al. 1999).

In the Red Sea Rift (RSR), where the axis is uniquely characterized by a line of bathymetric lows known as “Deeps” (Bäcker and Schoell 1972), the transition from rifting to spreading has been proposed to occur concurrently at several “nodes” (marked by the Deeps, see also Fig. 1) scattered over the 670 km-long region between 19.5°N and 24°N (Bonatti 1985). The relative proximity of the Red Sea rift to the Arabian/Nubian plate Euler pole results in significant variations in spreading rate over this distance which in turn implies that, if the “nodes” idea is correct, spreading must have initiated after varying amounts of continental stretching. Propagation of the “nodal” spreading centres into the intervening continental blocks has been proposed to eventually lead to continental break-up (Bonatti 1985; Cochran 2005; Ligi et al. 2012). However, most of this Red Sea tectonic interpretation is based on bathymetric and geophysical data collected prior to 1990, with either large line spacing, relatively low spatial resolution and/or with questionable navigational accuracy.

We present here new high-resolution bathymetric data of the central Red Sea axis combined with backscatter information and ground-truthing. We use this data to study in detail the Red Sea axis, its volcanic and tectonic processes, nature of the inter-trough zones between the deeps and the transition from rifting to spreading in the Red Sea to develop a modern model for the Red Sea. We interpret the data as showing that the flow of submarine salt glaciers (namakiers) strongly influences rift morphology and that the spreading “nodes” merely represent regions of a continuous spreading axis not covered by salt, obviating the need for a special rifting/spreading transition mechanism for the Red Sea.

2 Geological Background

The Red Sea Rift (RSR) developed during the counter-clockwise rotation of Arabia from Nubia (Fig. 1; Girdler and Underwood 1985; Sultan et al. 1993; Cochran 2005). It is an ultraslow-spreading rift with current spreading rates between $\approx 10 \text{ mm yr}^{-1}$ in the northern Red Sea and 15.5 mm yr^{-1} in the central Red Sea (Chu and Gordon 1998; DeMets et al. 2010). In this respect, the RSR is comparable, for example, to the Southwest Indian Ridge ($12\text{--}16 \text{ mm yr}^{-1}$) or the Gakkel Ridge ($11\text{--}12 \text{ mm yr}^{-1}$; DeMets et al. 2010).

The oldest seafloor presently known in the axial trough occurs at 17°N and has been assigned an age of 3–5 Ma (Cochran 1983; Gurvich 2006). Older oceanic crust may be present under a blanket of thick sediments on the shelves of the main trough, and it has been proposed that oceanic seafloor spreading may have begun as early as 10–12 Ma (Izzeldin 1987; Augustin et al. 2014, 2016). The sediment cover consists of Miocene evaporites and younger pelagic carbonate ooze, with an estimated overall thickness of up to 7 km (Girdler and Styles 1974; Searle and Ross 1975). Continental break-up, rifting and seafloor spreading caused the kinematic deformation of these evaporites, that in some places have been shown to flow toward the deeper axial rift in the form of salt glaciers, known as submarine namakiers (e.g., Figs. 2, 3, 4, 5, 6; Girdler 1985; Mitchell et al. 2010; Augustin et al. 2014).

In the southern part of the Red Sea (south of 19.5°N) the axial valley is continuous and well developed. It is characterized by the distinct normal-fault-related axis-parallel bathymetric lineations and volcanism seen at other oceanic spreading centres (Gurvich 2006). Between 19°N and 23°N, oceanic volcanics only crop out in the Deeps, which form partially disconnected large basins (Bonatti 1985; Cochran 2005; Ligi et al. 2012). Further north, these Deeps are more widely spaced but at least three of them (Bannock, Mabahiss and Shaban) have been reported to contain basalt (Bonatti et al. 1984; Pautot et al. 1984; Guennoc et al. 1988). All basaltic samples so far recovered from all axial Deeps have been characterized geochemically as typical (for slow spreading) tholeiitic mid-ocean ridge basalts derived from a pure asthenospheric source with no indication of continental input (Altherr et al. 1990; Haase et al. 2000; van der Zwan et al. 2015).

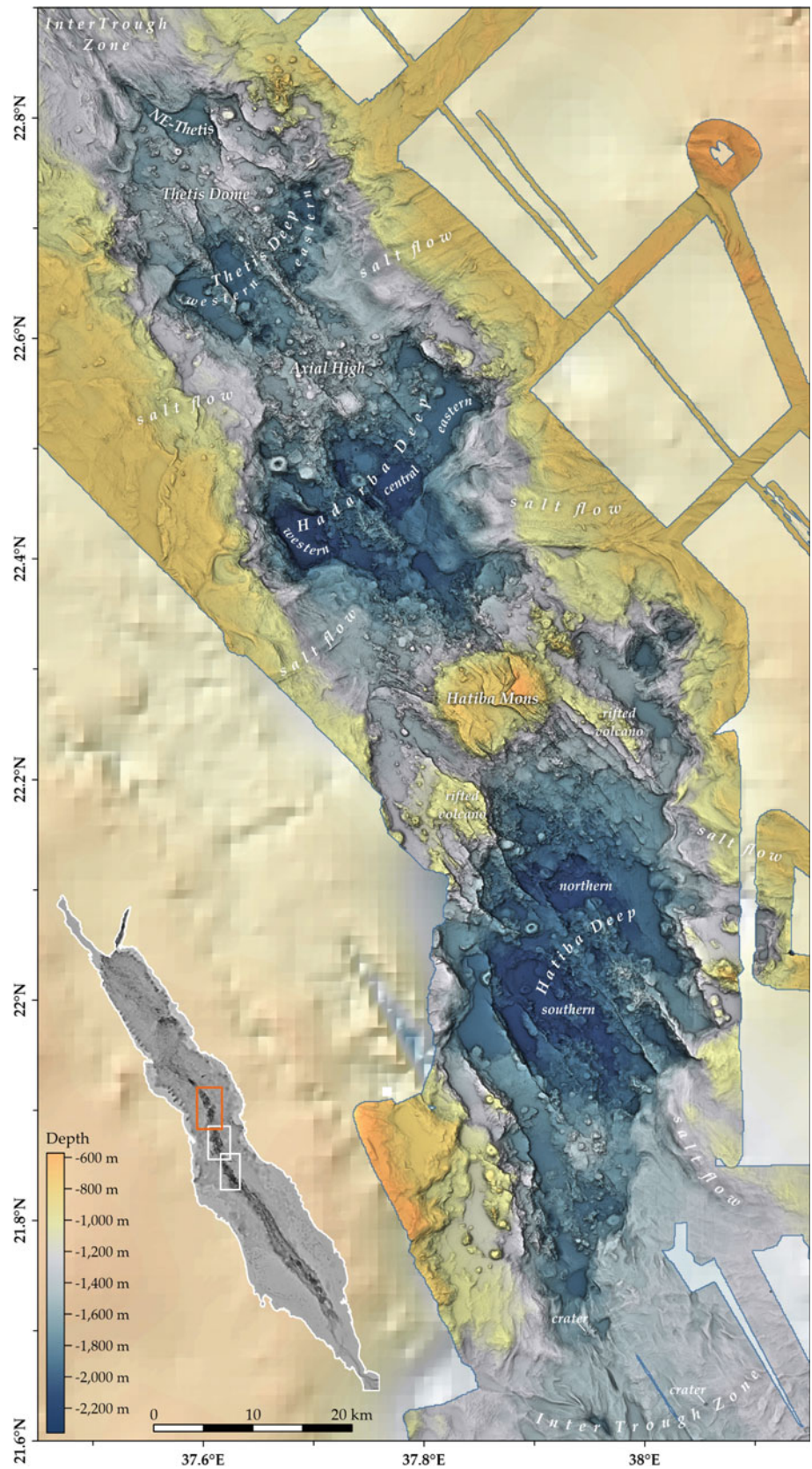
The Deeps are separated by so-called Inter-Trough Zones (ITZ; Figs. 1, 2, 4, 5, 6), which, as well as being shallower, are distinctly different in their geophysical characteristics (mainly gravity and magnetic) compared to the Deeps (Tramontini and Davies 1969; Searle and Ross 1975; Ligi et al. 2012). This led to them being interpreted as thinned continental crust and the widely accepted theory that the Red Sea Deeps are discrete axial spreading “nodes” (Bonatti 1985). Other authors (e.g., Searle and Ross 1975; Girdler and Whitmarsh 1974; Girdler 1985; Girdler and Evans 1977; Izzeldin 1987; Sultan et al. 1992; Augustin et al. 2014, 2016) have discussed the possibility that oceanic crust is present along the entire Red Sea axis but covered in large parts by laterally slumped evaporites and sediments; this alternative interpretation is recently supported by the newly available high resolution multibeam maps and seismic data (e.g., Mitchell et al. 2015; Augustin et al. 2014).

3 General Morphology and Segmentation of the Volcanic Ridge

Prominent first-order features of the Red Sea bathymetry are two major types of seafloor, distinguishable by their average rugosities. These are (I) relatively rugose regions, mainly comprising the Deeps and their immediate surroundings. These areas consist of a series of deep basins (the Red Sea Deeps) cross-cut by volcanic ridges and highs and divided by the ITZs, described in more detail below from N to S, and (II) comparatively smooth regions on the graben flanks and in the ITZs, identified and discussed in detail by Mitchell et al. (2010), Mitchell and Park (2014) and Augustin et al. (2014) as being the result of downslope flows of submarine namakiers.

The regions of the RSR that are not covered by namakiers and that represent the rugose regions show volcanic and tectonic features that are familiar structures on other slow- and ultraslow-spreading ridges (Dick et al. 2003; Cannat et al. 2009; Carbotte et al. 2015). For example, the RSR shows a clear rift valley with numerous volcanic edifices and axial volcanic ridges (AVRs). The partially overlapping AVRs mark the rift axis and split the rift valley into several basins, often bordered by salt flows. In the older low-resolution (>800 m) bathymetric data these basins have been highlighted as the “Deeps” and interpreted as oceanic spreading nodes. The new data shown in Figs. 2, 3, 4, 5, 6 clearly shows that the “Deeps” are analogous to common morphologic features of ultra-slow spreading rifts, related to segmentation by second order (non-transform) offsets. Large axial domes and volcanoes mark the centres of the second order segments, which tend to deepen toward the segment ends and form deep rifts parallel to semi-circular basin structures, typical for slow and ultraslow-spreading ridges (Carbotte et al. 2015). Ultraslow spreading ridges have few, if any, transform faults (they are, for example, absent on the 1900 km-long Gakkal Ridge and along the 1000 km-long segment of SWIR east of the Melville FZ; see also GEBCO or Sandwell et al. (2014) data sets). Except for the Zabargad fracture zone, transform offsets also appear to be absent along the 600 km-long portion of RSR studied here, as characteristic spreading-perpendicular valleys offsetting the rift axis with large-displacement (>30 km) are absent. This is in direct contrast to the large fracture zones or transform faults which have been proposed in the Red Sea by numerous authors (Coleman 1973; Coleman and McGuire 1988; Ghebreab 1998; Almalki et al. 2015; Schettino et al. 2016), that are based on land observations and free-air gravity data but for which, however, no evidence can be found in the bathymetry in form of rift perpendicular graben

Fig. 2 Bathymetric map of the Thetis–Hadarba–Hatiba Trough, hosting the Thetis Dome and Hatiba Mons volcano. High-resolution data (30 m) from the Urania RS05, Poseidon P408 and Pelagia 64PE-350/351 expeditions. Low-resolution background data: GEBCO. Projection is Geographic WGS84. Reprinted from Augustin et al. (2016) with permission of Elsevier



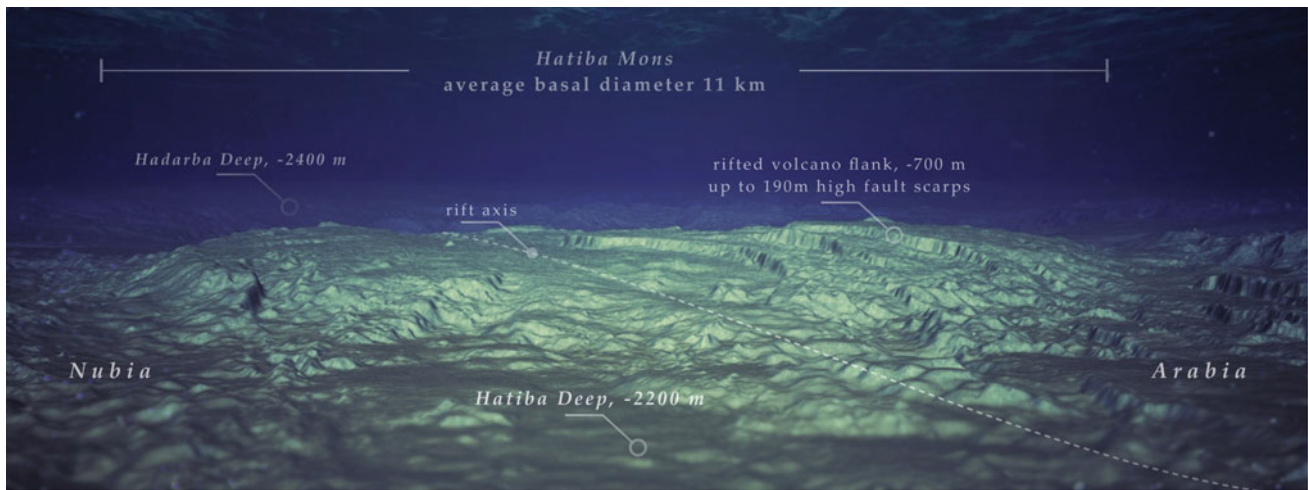


Fig. 3 3D-Visualization (Natural Scene Designer Pro 6 rendering) of Hatiba Mons, the largest axial dome volcano of the central Red Sea Rift. The picture simulates the view of the volcano toward the north.

High-resolution data (30 m) from the Urania RS05, Poseidon P408 and Pelagia 64PE-350/351 expeditions

structures that offset the ridge axis, flexure ridges or other morphological features known from transform faults (e.g., Carbotte et al. 2015). The latest bathymetry data revealed that the rift axis in the central RSR instead consists of a sequence of curvilinear second-order segments building one super segment extending 800 km from the Zabargad Fracture zone to the Danakil Triple Junction (see Fig. 1).

4 The Northern Deeps: Thetis–Hadarba–Hatiba Trough

The Thetis–Hadarba–Hatiba Trough consists of four major Deeps and basins along with several smaller basins, bordered by ITZs in the north and south and flanked by submarine namakiers (Mitchell et al. 2010; Augustin et al. 2014). The major Deeps and basins, namely NE-Thetis, Thetis, Hadarba and Hatiba (Figs. 1 and 2), are morphologically separated by three axial highs of which two are characterized by large dome-shaped volcanoes (Thetis Dome, Hatiba Mons). The Thetis Dome is a NW–SE (ridge parallel) faulted axial volcano with an average diameter of 11 km and a height of about 400 m. Despite the faulting that indicates the long history of the volcano, the Thetis Dome shows volcanic activity in backscatter and bathymetry data. Strong backscatter response (indicating hard, non-sedimented seafloor; Augustin et al. 2014), low seafloor ruggedness of these areas and the recovery of unaltered basalts (Bonatti et al. 2005; Ligi et al. 2012) indicate the presence of lava flows that are likely younger than 10 ka. Due to the high average sedimentation rates of 10 cm/ka in the Red Sea (Stoffers and Ross 1974) older lava flows would have been covered by too much sediment to be distinctively

visible in the backscatter data (Mitchell 1993; Hewitt et al. 2010). These lava flows run downslope north and south from the central graben into the NE–Thetis basin and the Thetis Deep (Augustin et al. 2016). The Thetis Dome is beset by a few small volcanic edifices and crossed by an axial volcanic ridge (AVR) that runs ridge parallel from the Nereus–Thetis ITZ toward the axial high that separates the Thetis and Hadarba Deeps, thereby splitting the Thetis Deep into two sub-basins (Fig. 2). Both sub-basins have a generally flat seafloor but show high backscatter areas and some volcanic cones and hummocks, and thus were volcanically active in Holocene times (<10 ka). The axial high at 22.5°N is covered with numerous volcanic hummocks, small flat-top volcanoes and domes with diameters of mostly <1 km. This volcanic high is also rift-parallel faulted and shows higher backscatter reflectivity only at the eastern side, suggesting relatively low recent volcanic activity.

The Hadarba Deep, south of the 22.5°N axial high, is 400 m deeper than the Thetis Deep and comprises three sub-basins, separated by AVRs. Volcanic activity, indicated by high backscatter, is concentrated along a prolongation of the NW–SE striking AVR from the Thetis Deep. West of this AVR we see a ridge jump represented by a second ridge-parallel AVR, which fades southward into the axial high topped by the Hatiba Mons volcano (11.4 km base diameter, 530 m high; Fig. 3). The northern end of this ridge is characterized by larger flat-top volcanoes with diameters of up to 3 km (Fig. 2). Along this AVR high backscatter signals and fresh lavas, with little grade of seafloor alteration, are only recovered from the southern end of the Hadarba Deep.

Hatiba Mons is (particularly on its eastern flank) faulted along a NW–SE strike, with minor cross cutting faults

Fig. 4 Bathymetric map of the Red Sea Rift at the Atlantis II Deep area and the Shagara–Erba Trough, hosting the Aswad Dome volcano. High-resolution (30 m) data from the Poseidon P408 and Pelagia 64PE-350/351 expeditions. Stars indicate the positions of off-axis highs that obstruct namakiers corresponding to VGG panel A in Fig. 7. Low-resolution background data: GEBCO. Projection is Geographic WGS84. Reprinted from Augustin et al. (2016) with permission of Elsevier

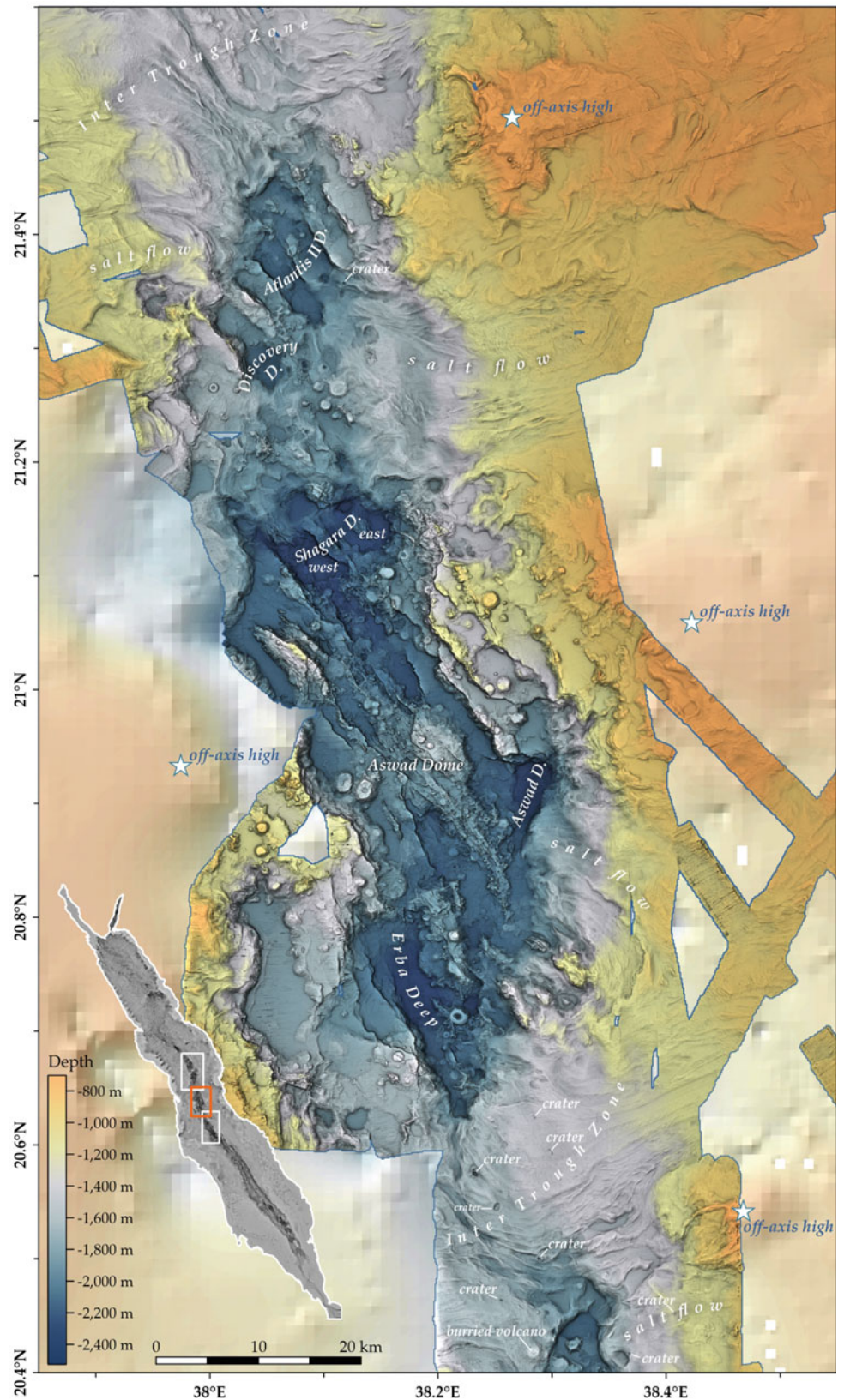
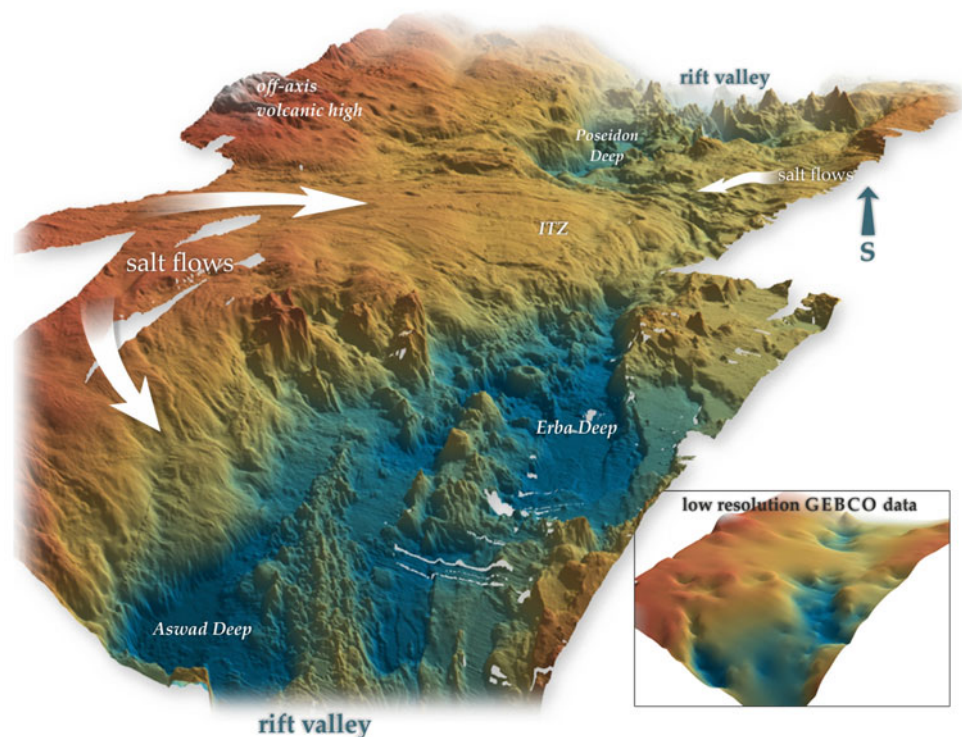


Fig. 5 3D-visualization of the large salt glacier that flows toward the Erba–Poseidon ITZ, creating a significant piedmont-lobe on the rift valley floor. The salt flows are influenced and redirected by volcanic structures. High-resolution data from the Poseidon P408 and Pelagia 64PE-350/351 expeditions. View direction to the south; the low-resolution GEBCO data of the same area is shown for direct comparison. After Mitchell and Augustin (2017) with permission of Elsevier



striking SW–NE. Small satellite cones and hummocky volcanic features are situated at the rim of the main structure. Areas with high backscatter reflectivity along the southern volcano flank, originating from the topographically smooth central part, suggest geologically recent lava flows. This is comparable to the lava flows described from Thetis Dome above. Distinct morphologic highs SW and SE of Hatiba Mons, sharply cut by normal faulting toward the rift valley, suggest a precursor volcanic structure of the recent edifice (marked as “rifted volcano” in Fig. 2).

South of Hatiba Mons lies the 25 km-wide and 60 km-long Hatiba Basin, which is divided by NW–SE striking AVRs and faults into north-eastern and south-western basins. Volcanic hummocks and small flat-top volcanoes are scattered all over the Deep, but are not as abundant as in the Thetis and Hadarba Deeps. High backscatter reflectivity in the northern Deep seems to be directly connected to the lava flow originating from Hatiba Mons. Sampling of high backscatter areas in the deepest area of the southern Deep recovered unaltered basalts. These basalts show sediment filled enclosed pockets as well as irregular, lobate flow patterns indicating that the lavas may have sunk into a soft base. This suggests that the lavas erupted onto a wet sedimented environment. The other parts of the basins as well as adjacent terraces show low backscatter intensities and, based on gravity coring results, are covered by at least 2 m thick sediments (Schmidt et al. 2011). Toward the southwest the Hatiba Deep is flanked by

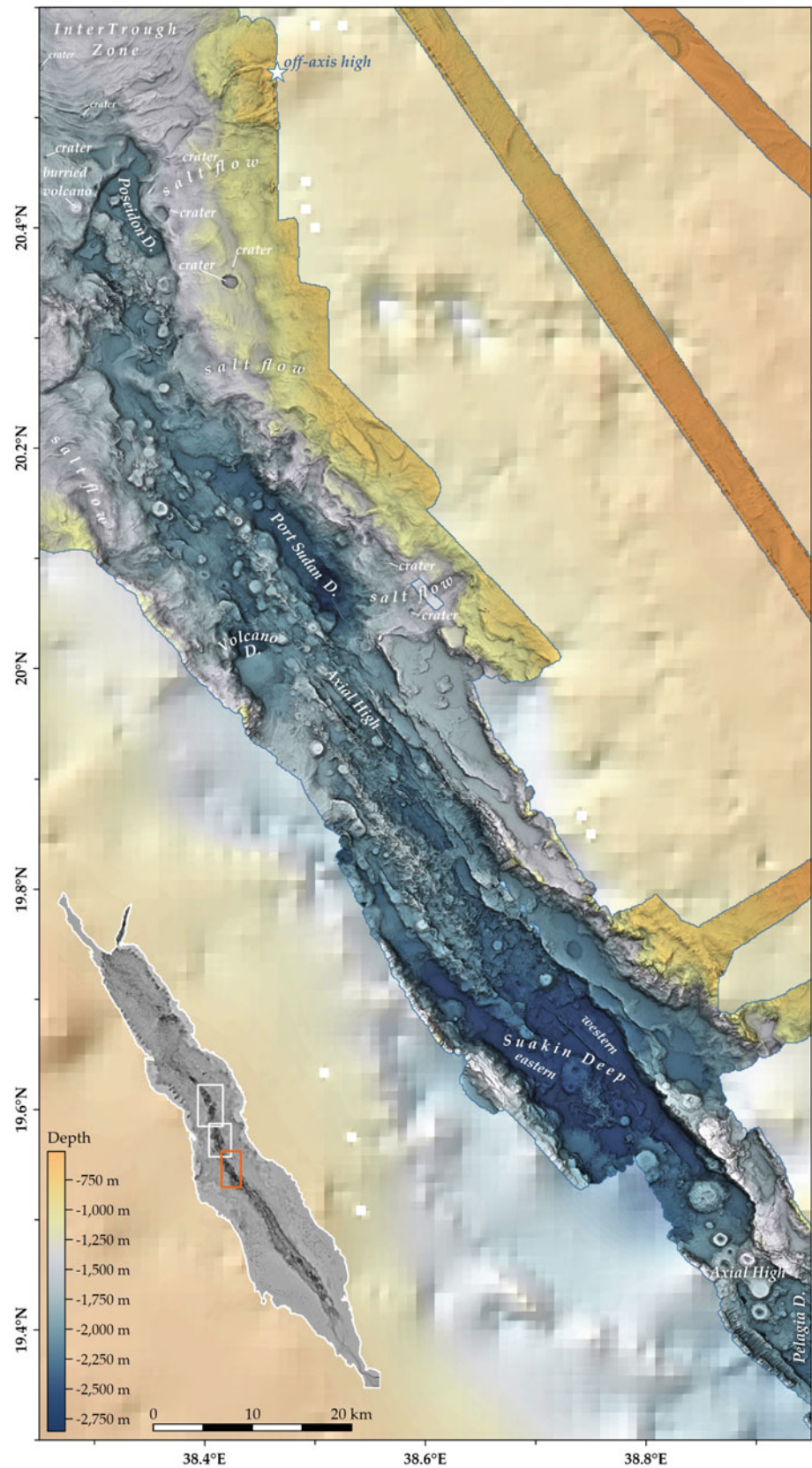
uplifted terraces with scattered volcanic edifices and is bordered to the south by an ITZ.

5 Atlantis II Deep Area and the Shagara–Aswad–Erba Trough

The Atlantis II Deep marks the northernmost end of the Atlantis II–Shagara–Erba Trough section, hosting also numerous sub-deeps, for example, the Discovery and Aswad Deeps (Figs. 1 and 4). The Atlantis II Deep area has been subject to many studies since the 1960s because of the presence of hot brine pools that contain economically valuable metalliferous sediments (Gurvich 2006, and references therein). In general, the area of the Atlantis II Deep appears smoother in bathymetry and less rugged than the basins north and south of it, which is due to massive inflows of salt and sediments from nearly all sides into the Deep (Augustin et al. 2014; Feldens and Mitchell 2015). Clearly visible in the bathymetry are the NW–SE-striking normal faults, tilted blocks and the “central sill” of the Deep described in earlier works (Bäcker and Richter 1973). Only a few prominent volcanoes south of the Atlantis II Deep and west of the Discovery Deep (partially overflowed by namakiers) and little hummocky volcanics are visible in the bathymetry.

The smooth terrain with adjacent namakiers develops southward into the rougher and deeper terrain of the

Fig. 6 Bathymetric map of the Red Sea Rift from the Poseidon Deep to the Pelagia Deep. High-resolution data (30 m) from the Poseidon P408 and Pelagia 64PE-350/351 expeditions. The star indicates the position of an off-axis high that obstructs namakiers corresponding to the southernmost high shown in VGG panel A in Fig. 7. Low-resolution background data: GEBCO. Projection is Geographic WGS84. Reprinted from Augustin et al. (2016) with permission of Elsevier



Shagara–Aswad–Erba Trough. This 65-km long trough is marked by steep very sharp normal faults and is roughly divided by a central 28 km long and 5 km wide AVR into two elongated axis parallel basins (Shagara–Aswad and Erba). This AVR also crosses a strongly faulted central dome volcano that separates the Shagara and Aswad Deeps (Aswad Dome, ≈ 8.4 km in diameter, 470 m high; Fig. 4). Flat-top volcanoes and hummocks are abundantly found on the faulted Aswad Dome and backscatter data indicates Holocene volcanic activity at its axial areas, although less than at Hatiba Mons and the Thetis Dome.

Also in the Shagara Deep, a ridge-parallel AVR separates the Deep into two basins that have a flat seafloor and contain metalliferous sediments. The SE flank of the Shagara Deep shows numerous scattered volcanoes and hummocks on an elevated terrain. Terraces east and west of the Aswad Dome are uplifted to water depths of less than 1200 m and are again scattered with numerous flat-top volcanoes and some hummocky volcanic ridges and edifices. The Aswad Deep (situated east of the Aswad Dome; Pautot et al. 1984; Blanc et al. 1990) is a rather smooth, NE–SW striking basin, but is also volcanically active as indicated by bright backscatter and fresh basaltic glass recovered from its southern part (Schmidt et al. 2013; van der Zwan et al. 2015).

The Erba Deep is situated 15 km south of the Aswad Dome (Gurvich 2006, and references therein; Fig. 2). A NW–SE striking AVR, hosting some flat-top volcanoes and the adjacent flat basin are its main features. Backscatter data as well as the dredging of unaltered basalts revealed volcanic activity in the Erba Deep that might be younger than 10,000 years (van der Zwan et al. 2015). West of the Erba Deep large, ≥ 10 km wide and at least 25 km south trending, sedimented terraces with minor volcanic edifices are dominant. The terraces and the Erba Deep are bordered by namakiers at the westernmost edge of the dataset and in the south by a large piedmont-lobe-like namakier that forms the ITZ toward the southern Deeps (Figs. 4 and 5; Augustin et al. 2014; Feldens and Mitchell 2015).

6 Poseidon, Port Sudan, Suakin and Pelagia Deeps

Between 20.2°N and 20.5°N only a 5–10 km wide and about 30 km long section of the RSR ocean crust outcrops between the salt-covered flanks, consisting of the Poseidon Deep at its northern end (Figs. 1, 5 and 6; Augustin et al. 2016). Backscatter data indicates volcanic activity within the Poseidon Deep and at its eastern flanks. Massive inflows of salt and sediments from both rift flanks and from the north partly cover the AVRs, volcanic edifices and boundary faults (Figs. 1 and 6; Augustin et al. 2014). For example, south of

the Poseidon Deep a NW–SE striking ridge of hummocky volcanic edifices, flanked by some flat-top-volcanoes, is crosscut by namakiers in the north and south, while at the north-western edge the shape of an underlying single flat-top volcano can be traced through the evaporite cover. Remarkable is the fact that just north of this ridge recent lava flows seem to originate from the eastern namakiers and run toward the Poseidon Deep as visible in backscatter data (Augustin et al. 2014). A prominent 1.5 km wide and 150 m deep crater structure with a surrounding 20–30 m high ring mound is situated about 5 km southeast of the Poseidon Deep within a namakier (Fig. 6). Numerous comparable but smaller and slightly deformed structures are found within the ITZs.

South of $\sim 20.2^\circ\text{N}$ the RSR axis widens to ≥ 20 km. A straight NW–SE-running AVR separates the Port Sudan Deep in the east from the shallower Volcano Deep in the west (Pautot et al. 1984; Blanc et al. 1990). A 4 km large, smooth, dome-shaped volcano, that is partially covered by namakiers, comprises about two thirds of the Volcano Deep. Recent, <10 ka volcanism in both Deeps is inferred by sampling of unaltered basalt and/or backscatter data although the Port Sudan Deep is also partially filled with hydrothermal sediments (Schmidt et al. 2013; van der Zwan et al. 2015).

South of the Volcano and Port Sudan Deeps the separating hummocky, volcanic ridge continues as a heavily NW–SE faulted discreet axial high at 19.9°N. This high is flanked in the west by inflowing sediments and in the east by a large ≥ 5 km wide and 35 km long NW–SE trending terrace. As an extension of the 19.9°N axial high a 35 km long and up to 10 km wide AVR runs southward to the Suakin Deep, where it continues, less obviously, as a chain of axial hummocks, flat-top and small dome-shaped volcanoes that divide the Suakin Deep into an eastern and a western basin (Fig. 4). The Suakin Deep marks the deepest part of the Red Sea (2860 m), and no signs of recent volcanic activity, either in backscatter data or in rock sampling, could be found. The few recovered basaltic samples show up to cm-thick carbonate and/or manganese encrustations, not visible in the backscatter data and implying an older age (see also Schmidt et al. 2013; van der Zwan et al. 2015). Distinct uplifted terraces with a smooth morphology border the Deep to the east. South of the Suakin Deep at 19.4°N another axial high occurs, which is beset with several flat-top volcanoes and reveals bright backscatter signals, suggesting extensive recent volcanic activity. The axial high is followed by the Pelagia Deep (Augustin et al. 2016), which is a 16-km long basin that marks the geomorphological change from a Deeps-and-Basin morphology to a 300 km-long section of uninterrupted volcanic seafloor with a more constant morphology that is considered as the matured rift (Bonatti 1985).

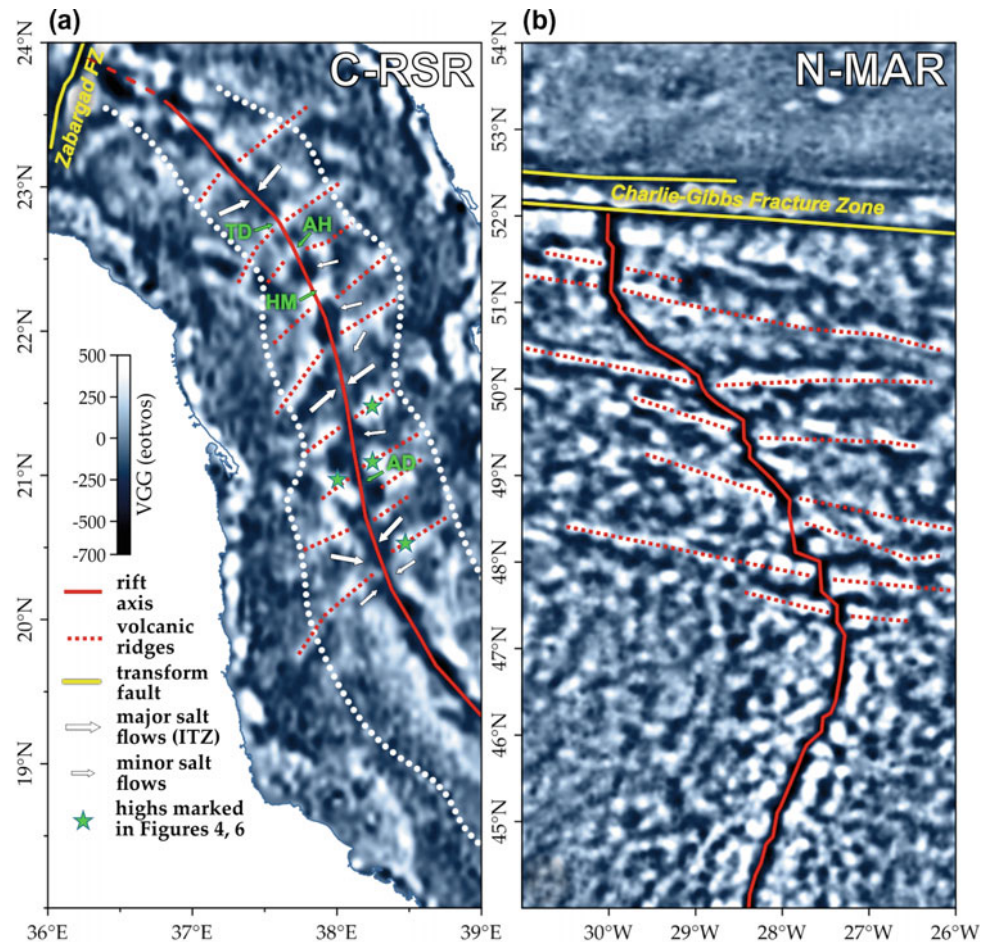
7 Volcanic Ridges and the Age of the Oceanic Crust

A particular feature of the Red Sea that was not recognised in earlier times is the occurrence of large dome-shaped volcanoes and axial highs. These are a typical feature of (ultra) slow-spreading ridges, where long-term focussed magmatic activity at segment centre highs and domes can be traced over large distances (Cannat et al. 2009; Carbotte et al. 2015). The result is that along (ultra)slow-spreading ridges, spreading-perpendicular volcanic lineaments can be found in bathymetry and gravity data. In the Red Sea, these ridges are partially covered underneath the namakiers, but visible in both the vertical gravity gradient (VGG) and free-air gravity data between 20°N and 23°N. Although this is a simplified interpretation of VGG and free-air gravity data, the large-scale patterns reveal, in addition to ridges adjacent to the three large dome-shaped volcanoes discussed above, at least six other spreading-perpendicular ridges in the central Red Sea (Fig. 7a; Sandwell et al. 2014; Mitchell and Park 2014). The gravity patterns look like those from, for example, the northern MAR (Sandwell et al. 2014; Fig. 7b) but appear less crisp, thus representing a comparable oceanic crust under the thicker Red Sea sediments and salts.

These volcanic ridges appear to span 100–170 km and extend from the ridge axis toward the maximum reach of continental crust as described by Izzeldin (1987), suggesting that the volcanic ridges had a very stable magma production with seafloor spreading over a long interval. As this continental reach is at a distance of 60–180 km from the escarpments, this fits well with a breakup of the continent after total stretching of 200 ± 40 km as given by Taylor et al. (1999), White and McKenzie (1989) or Grachev (2003). Spreading ages (distance from ridge axis times half the spreading rate) of the spreading-perpendicular ridges vary from about 8–9 Myr at the Nereus and Thetis Deeps, up to 12 Myr at the southernmost ridge identified in the VGG (at 20°N, Poseidon Deep area) (Fig. 7a; spreading rates after Chu and Gordon 1998). The calculated spreading ages are related in resolution to the spatial resolution of the used datasets but agree very well with the 8–12 Myr of oceanic spreading discussed by Izzeldin (1987) and Augustin et al. (2014).

The rift-perpendicular ridges disappear south of 20°N, where the character changes from patchy to ridge parallel in VGG-patterns, comparable to other mid-ocean ridges where segmented and unsegmented crust alternate in unequal proportions (Fig. 7a). The absence of spreading-perpendicular ridges in the southern Red Sea was discussed by Mitchell

Fig. 7 Vertical gravity gradient (VGG, after Sandwell et al. 2014) of (a) the central Red Sea compared to (b) the northern Mid-Atlantic Ridge. The comparison shows that the VGG data reveal hidden spreading-perpendicular volcanic ridges (dashed lines) under the sedimentary cover that are comparable to those at the N-MAR. The ridges visible in the Red Sea VGG influence the direction of submarine salt flows (arrows) and end at the maximum extent of continental crust (white dotted line; Izzeldin 1982). Stars mark large off-axis volcanic highs that influence the salt flows and are clearly visible in the bathymetry. TD = Thetis Dome, AH = axial high, HM = Hatiba Mons, AD = Aswad Dome. Projection is Geographic WGS84. After Augustin et al. (2016) with permission of Elsevier



and Park (2014) as being the result of the rising influence of the Afar plume, which is comparable to the Reykjanes Ridge (MAR) where (due to the Icelandic plume) such patterns are absent as well.

8 Inter-trough Zones and Namakiers

In contrast to the volcanic Deeps, the inter-trough zones show significantly lower average rugosities and shallower average depths (1300–1600 m; Figs. 2, 3, 4). The seafloor in the ITZs is, however, not completely smooth, and long-wavelength (relative to the hummocky terrain in the Deeps) linear ridges are visible in many regions. These appear to be flow-structures described by Mitchell et al. (2010) and Augustin et al. (2014) interpreted as resulting from flow in salt, producing salt glaciers (namakiers). The local topographic slope and the orientation of the longitudinal ridges and troughs on the surfaces of the namakiers allow a sense of flow to be determined (Figs. 2 and 3). Where two namakiers collide that flow from opposite sides into the rift, a central cleft or suture is generally visible where the rift axis is covered (Augustin et al. 2014). The bathymetric data also show that namakier flows are affected by the underlying topography as they apparently deviate around volcanoes and volcanic ridges on the rift flanks. The distribution of the large namakier movements, that build up the ITZs, seems also to be strongly influenced by the underlying topography and particularly influenced by the rift-perpendicular volcanic ridges (in VGG), as can be seen by comparing the locations of these ridges to the occurrence and flow directions of namakiers (Fig. 7a; Mitchell and Augustin, in preparation). We observe that the major namakiers which completely blanket the RSR in the ITZs flow toward the rift in the regions between the spreading-perpendicular volcanic ridges. In several cases, higher terrains of volcanic ridges prevent the salt from completely covering the axial rift (marked by stars in Figs. 4, 6, 7a). This explains at least some of the flow directions as seen in bathymetric data (Mitchell et al. 2010; Augustin et al. 2014; Feldens and Mitchell 2015) and why the ITZs and the “Deeps” are where they are.

9 The Nature of the Crust and Volcanism Below Submarine Namakiers

As namakiers blanket the ITZs, conclusive evidence on the subsurface beneath them is difficult to obtain. However, as discussed above, several structures within the namakier give indications that the ITZ subsurface is volcanic and similar to the oceanic rift. At the flow fronts we see linear volcanic ridges apparently being overflowed by the namakiers. These

irregular, non-tectonic but sharp contacts suggest an on-lap situation. In some cases, a continuation of the ridge beneath the namakier can be discerned. This is, for example, the case in the Poseidon Deep, where a NNW–SSE striking ridge terminates against the northern namakier but a circular, flat-topped structure, similar in size to an axial flat-top volcano, is visible in the bathymetry of the namakier, probably indicating a covered volcano (Fig. 6). A continuation of volcanic features deep into an ITZ is also apparent where namakiers do not yet completely blanket the rift. For example, small volcanoes can be observed as far as 10 km onto the ITZ south of the Nereus Deep in the still-open ITZ suture (Augustin et al. 2014). These features can be taken as evidence that the oceanic rift is continuous underneath the ITZs and is merely blanketed, rather than being continental crust (Augustin et al. 2014).

Thus, the unique combination of evaporites covering an active rift results in specific features. Within the Nereus–Thetis ITZ and Erba–Poseidon ITZ as well as south-east of the Poseidon Deep we discovered crater structures, often with elevated rims (10–25 m above the surrounding surface; Figs. 1, 2, 4 and 6). The size of the craters varies from 450 m to 1700 m in diameter with a depth of 50 m to 150 m respectively (average aspect ratio is 0.08; Augustin et al. 2016).

An origin of these craters as the formation by karst-like dissolution of salt caused by penetration of seawater, or by dissolution/distortion of salt from the base by escaping gases and/or hydrothermal fluids venting from oceanic crust, can be excluded due to geomorphological misfits and the specific local geological settings of the craters (Augustin et al. 2016). The salt-craters are all located in areas where namakiers are interpreted to overlie the neo-volcanic zone or volcanically active parts near the axial valley (Figs. 1, 2, 4 and 6). This, together with the shape of the craters and the presence of elevated rims around the craters that resemble maar craters on land (Büchel 1993; Geshi et al. 2011), suggests that the craters may be the result of phreatic or phreatomagmatic explosions caused by magma intrusions at or above the basement/salt boundary (Walker 1973; Sato and Taniguchi 1997). Phreatomagmatic eruptions would require that water reaches the base of the namakiers through the pelagic sediment and salt layers. Although little is known about the rheology and permeability of submarine namakiers the penetration of water into and under the salt bodies along faults and basaltic dikes is probable, considering the extensional tectonic setting of the area (e.g., Mitchell et al. 2010; Guennoc et al. 1988; Ross and Schlee 1973). Furthermore, hydrothermal recharge, passing the evaporites, is indicated by evidence for highly saline evaporitic fluids being added to Red Sea magmas (van der Zwan et al. 2015). Therefore, the presence of highly saline pore waters and trapped brines within or at the base of the evaporite sequences is at least

locally plausible. Schofield et al. (2014) reported on non-brittle emplacement of magma and magma-salt mingling from the Herfa-Neurode mine (Germany), possibly by melting of salt (melting point of NaCl ≈ 800 °C, hydrous salts < 200 °C; Driesner and Heinrich 2007; Schofield et al. 2014). This indicates that intrusions of about > 1000 °C (Moore and Evans 1967) tholeiitic magmas (with normal to enriched trace-element compositions, as typical for the Red Sea Rift; Altherr et al. 1988) into a submarine namakier that contains comparable salt assemblages (Manheim et al. 1974; Stoffers and Kühn 1974) most likely melts the surrounding salts and heats up saline fluids significantly. Temperatures of ≥ 400 °C already vaporize any saline fluids within the salt and trapped below (at pressures of ≈ 300 bar, e.g., Driesner and Heinrich 2007). Girdler and Whitmarsh (1974) and Girdler (1985) discussed the role of namakiers as thermal insulators. The namakier blanketing could slow down the cooling of magmatic intrusions. The magma is likely heating up and vaporizing significant amounts of the surrounding fluids and salt to build up sufficient steam pressure to blast away overlying salt and sediments by phreatic eruptions at the seafloor. Thus, the observed craters are likely the product of such eruptions and these craters indicate places of the oceanic crust where volcanism has taken place after these were covered by the salt. Using these craters, we can track the occurrence of oceanic crust also underneath the salt cover.

10 Root Zones and Volumes of Submarine Namakiers

Next to the namakier-covered ITZs we find that the rift flanks are somewhat deeper than the general flank depth, and are characterized by large semi-circular 100–150 m deep embayments (Fig. 8). These depressions east and west of the rift valley likely represent the root zones of the valley-filling namakiers. To test this, Augustin et al. (2014) estimated the volumes, which (I) would be needed to fill up the rift valley and (II) are represented by the missing material from the embayment depressions.

The results of these calculations are shown in Fig. 8 for the ITZs between the Nereus and Thetis Deeps, the Hatiba and Atlantis II Deeps as well as for the namakiers which flow from the eastern flank into the Atlantis II Deep, and between the Erba and Port Sudan Deeps and the piedmont lobe flowing from the western rift-flank toward the Erba–Poseidon ITZ. The calculated loss and fill volumes for postulated namakier root zones and their rift filling are very similar (Fig. 8). Considering the uncertainties involved in estimating these volumes, we consider this close match to be strong supporting evidence for our assumption that the top of basement in the ITZs is a direct continuation of the

surrounding ocean crust–namakier contact, also confirming a continuous spreading rift.

We also calculated namakier thicknesses in the ITZ using this top-of-basement estimate (Fig. 8b–h). The Nereus-Thetis Deep ITZ namakier is the thickest, at up to 800 m calculated thickness (Fig. 8b and e), while the namakier flowing from the east toward the Erba–Poseidon Deep ITZ is, with 600 m, somewhat thinner (Fig. 8d and h). These estimates are significantly lower than the 4–5 km salt accumulations that have been estimated for ITZs from earlier seismic studies (Tramontini and Davies 1969; Ligi et al. 2012). The former study (Tramontini and Davies 1969) found a velocity in the Miocene evaporites in the range 4.2–4.6 km s⁻¹ based on seismic refraction. This velocity is similar to that reported for massive basaltic flow units from DSDP Hole 504B and IODP Hole 1256D (Little et al. 1985; Swift et al. 2008) and Tramontini and Davies (1969) noted that volcanic and evaporitic layers would most probably be seismically indistinguishable. Far more interesting is that Tramontini and Davies (1969) found what they termed a “lower layer” with a mean seismic velocity between 6.4 and 6.6 km s⁻¹ extending beneath both the Deeps and the ITZ at depths of 3–6 km below the sea surface. This velocity is typical of lower oceanic crust (Gilbert and Salisbury 2011; Carlson 2014), which might be expected at this depth but significantly higher than the 5.9–6.4 km s⁻¹ typically found in the upper 15 km of the Arabian Shield (e.g., Prodehl and Mechie 1991). This means that the earlier much thicker 4–5 km salt estimations may be the result of the similar salt-basalt velocity and rather represent the combined layer of the two, while the boundary shows the changeover to the lower oceanic crust. We take this as further evidence that the namakiers of the ITZs blanket oceanic crust.

11 Magnetic and Gravity Anomalies and Magnetic Quiet Zones

An important argument that has been previously advanced to support the presence of continental crust beneath the ITZ has been the absence of clear axis-parallel magnetic anomalies, which should be present if these areas were underlain by oceanic lithosphere. However, this argument seems to be negated by magnetic observations from the axial trough of the Red Sea itself. For example, the area between the Hadarba and Nereus Deeps (via the Thetis Deep), despite being unequivocally volcanic, shows an irregular intensity of magnetic anomalies and rock magnetization (Ligi et al. 2012), with only a diffuse and weak boundary (rather than a clear transition as would be expected from an ocean-continent transition) toward the non-magnetic appearance of the ITZ. Areas where Mitchell et al. (2010) and Augustin et al. (2014) described namakiers flowing

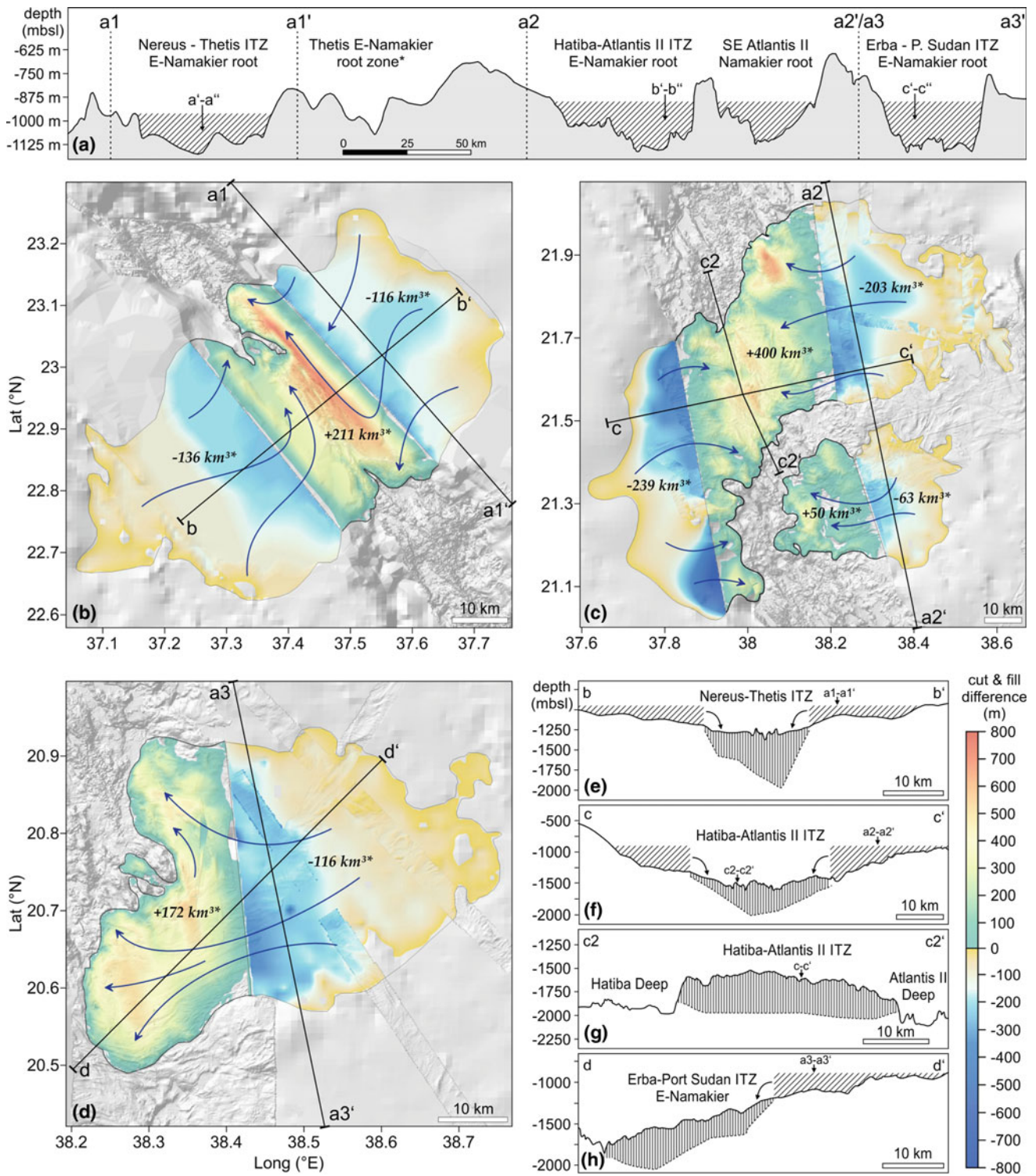


Fig. 8 Illustration of namakier source zones, calculated namakier volumes and depth of namakier–crust boundaries. **a** Bathymetric profiles over the western embayment depressions (profile a in **b**, **c**, **d**) showing the salt-loss regions (namakier sources). Hatched areas indicate loss-thickness. Positions of rift perpendicular profiles b, c, and d are shown by arrows. **b–d** Depths of the namakier source

embayments as well as the calculated thickness and volumes of the namakiers in the RSR (after Augustin et al. 2014). Arrows mark possible salt flow routes. **e–h** Across and along ITZ profiles (profiles b, c, c2, d in **b**, **c**, **d**) with modelled namakier–crust boundaries (dashed lines), showing the salt loss and fill areas. After Augustin et al. (2014) with permission of Elsevier

toward the RSR axial valley also appear low in magnetization. The large Hatiba Mons volcano, despite showing evidence for recent volcanic activity (Augustin et al. 2016), shows significantly lower magnetic anomalies and less rock magnetization than seen in parts of the Thetis and Nereus Deeps (Ligi et al. 2012). The tendency for volcanic complexes to have low or negative magnetic anomalies is known from other regions, for instance, the Palinuro Seamount in the Mediterranean Sea shows large regions with strong negative magnetic anomalies where hydrothermal alteration processes have played a relevant role (Caratori Tontini et al. 2009).

Blanketing of the neovolcanic zone by namakiers might significantly reduce the intensity of its magnetization. Magnetic “quiet zones” on sedimented spreading centres are well known from, for example, the Guaymas Basin (Gulf of California), the Escabana Trough (Gorda Ridge) and Middle Valley (Juan de Fuca Ridge) where they have been explained as resulting from enhanced hydrothermal alteration and the breakdown of magnetic minerals under the sedimentary blanket (Levi and Riddihough 1986). Girdler and Whitmarsh (1974) and Girdler (1985) calculated temperatures of up to 100 °C under the salt/sediment covers based on heat-flow measurements and discussed the role of evaporites as thermal isolators, inhibiting a significant magnetization of the oceanic crust under the ITZ.

The interaction between namakiers and the spreading system may be very important for the magnetic structure of the Red Sea Rift. Egloff et al. (1991) showed some magnetic anomalies (adapted from Izzeldin 1987) under the evaporite series west of the Suakin Deep. This Deep belongs morphologically to the continuous southern RSR (which begins roughly with the Port Sudan Deep at 20°N), which shows no interruptions by any ITZs. According to our model this would imply that, either because the spreading rate is too high (spreading velocities south of the Port Sudan Deep increase significantly toward a maximum at 18°N (12.5–16 mm yr⁻¹)) or namakier activity too low, the neovolcanic zone does not get covered in salt and only older, cold oceanic crust is buried. Heat flow in this older crust will be significantly lower than at the neovolcanic zone, possibly low enough that the thermal blanketing effect of the salt does not result in loss of magnetization.

The presence of gravity anomalies in, for example, the Thetis–Nereus or Hatiba–Atlantis ITZs (Searle and Ross 1975; Ligi et al. 2012) were also discussed as an argument for the presence of continental crust between the volcanic Deeps and troughs. Nevertheless, Searle and Ross (1975) showed that accumulation of sediments and salt could explain, for example, the 30 mGal difference in Bouguer anomalies observed between the Atlantis II Deep and the ITZ to the north, with no requirement for differences in the underlying crustal structure. This agrees with observations from the eastern Gakkal Ridge, for example, where the

active ridge is buried under terrigenous sediments, producing a distinct (free-air) gravity low of –20 to –50 mGal (Drachev et al. 2003) and from the Guaymas Basin (Gulf of California) where a salt body coincides with a (free-air) gravity low (Miller and Lizarralde 2013).

12 Conclusions

Based on the observations that we can make from the new bathymetric maps in combination with the given geophysical data and ground truthing we conclude that the Red Sea Rift shows characteristics that are very comparable to slow- and ultraslow spreading ridges elsewhere, but also some differences that can be attributed to the closeness of the Afar plume and the unique blanketing of the rift valley by large submarine namakiers:

- (I) Extensive salt flows (submarine salt glaciers or namakiers) are evident along the entire studied Red Sea Rift. In places, these namakiers flow into the axial region and completely blanket it while the flow directions are strongly influenced by the underlying basement topography. In the namakier covered areas, evidence from bathymetry, volume balance calculations of the salt flows, and geophysical data all seems to support the conclusion that the sub-salt basement is also basaltic in nature and represents oceanic crust.
- (II) Where not covered by namakiers, the volcanic seafloor comprises characteristics of a mid-ocean spreading axis. The large geomorphological structures such as, for example, a deep rift valley, steep faults, highly tectonized terrain, rifted volcanoes, bent volcanic ridges with overlapping spreading centres and second order non-transform offsets are typical for slow- and ultraslow spreading ridges elsewhere.
- (III) The unique occurrence of evaporites partially covering the active rift leads to distinct volcanic features. We see evidence for volcanic activity under the salt blanket in the form of explosion craters within the ITZ and at the graben flanks, as well as spots that indicate recent lava flows originating through the salt blankets and flowing into the rift valley. Thus, even though large parts of the oceanic crust are buried under layers of salt and sediments, recent volcanism can still be traced.
- (IV) Bathymetry and VGG data reveal traces of hidden rift perpendicular ridges under the salt, comparable to the volcanic ridges seen at other slow- and ultraslow spreading ridges. Spreading appears to have begun along the entire Red Sea axis at least as far north as the Nereus Deep at 23°N; these ridges indicate stable magma focusing and oceanic spreading since at least 12 Ma in the Red Sea.

Acknowledgements The authors would like to thank the captains, crews and scientific parties of the expeditions with R/V Poseidon P408 and R/V Pelagia 64PE350/351 as well as the student helpers at GEOMAR, Kiel, who helped in processing the huge amount of data. We kindly thank Marco Ligi for providing the Urania RS05 bathymetry grid. Saudi Geological Survey is thanked for inviting us to the Red Sea Book Workshop. The Jeddah Transect Project between King Abdulaziz University and Helmholtz-Centre for Ocean Research GEOMAR was funded by King Abdulaziz University, Jeddah, Saudi Arabia, under grant no. T-065/430.

References

- Almalki KA, Betts PG, Ailleres L (2015) The Red Sea—50 years of geological and geophysical research. *Earth-Sci Rev* 147:109–140
- Altherr R, Henjes-Kunst F, Puchelt H, Baumann A (1988) Volcanic activity in the Red Sea axial trough—evidence for a large mantle diapir? *Tectonophysics* 150:121–133
- Altherr R, Henjeskunst F, Baumann A (1990) Asthenosphere versus lithosphere as possible sources for basaltic magmas erupted during formation of the Red-Sea—constraints from Sr, Pb and Nd isotopes. *Earth Planet Sci Lett* 96:269–286
- Augustin N, Devey CW, van der Zwan FM, Feldens P, Tominaga M, Bantan RA, Kwasnitschka T (2014) The rifting to spreading transition in the Red Sea. *Earth Planet Sci Lett* 395:217–230
- Augustin N, van der Zwan FM, Devey CW, Ligi M, Kwasnitschka T, Feldens P, Bantan RA, Basaham AS (2016) Geomorphology of the central Red Sea Rift: determining spreading processes. *Geomorphology* 274:162–179
- Bäcker H, Richter H (1973) Die rezente hydrothermal-sedimentäre Lagerstätte Atlantis-II-Tief im Roten Meer. *Geol Rundsch* 62:697–741
- Bäcker H, Schoell M (1972) New deeps with brines and metalliferous sediments in Red Sea. *Nat Phys Sci* 240:153–158
- Blanc G, Boulegue J, Charlou JL (1990) Profils d'hydrocarbures légers dans l'eau de mer, les saumures et les eaux intersticielles de la fosse Atlantis II (Mer Rouge). *Oceanol Acta* 13:187–197
- Bonatti E (1985) Punctiform initiation of seafloor spreading in the Red Sea during transition from a continental to an oceanic rift. *Nature* 316:33–37
- Bonatti E, Colantoni P, Vedova BD, Taviani M (1984) Geology of the Red Sea transitional region (22°N–25°N). *Oceanol Acta* 7:385–398
- Bonatti E, Bortoluzzi G, Calafato A, Cipriani A, Ferrante V, Ligi M, Lopez Correa MCM, Redini F, Barabino G, Carminati E, Mitchell N, Sichler B, Schmidt M, Schmitt M, Rasul NRN, Al Nomani S, Bahareth F, Khalil S, Farawati R, Gitto D, Raspagliosi M (2005) Geophysical, geological and oceanographic surveys in the Northern Red Sea. Report on the morphobathymetric, magnetometric, oceanographic, coring and dredging investigations during cruise RS05 aboard R/V Urania. ISMAR Bologna Technical Report 94:1–40 Bologna, Italy
- Büchel G (1993) Maars of the Westeifel, Germany. In: Negen-dank JFW, Zolitschka B (eds) *Paleolimnology of European Maar lakes*. Springer, Berlin Heidelberg, pp 1–13
- Cannat M, Sauter D, Escartín J, Lavier L, Picazo S (2009) Oceanic corrugated surfaces and the strength of the axial lithosphere at slow spreading ridges. *Earth Planet Sci Lett* 288:174–183
- Caratori Tontini F, Cocchi L, Carmisciano C (2009) Rapid 3-D forward model of potential fields with application to the Palinuro Seamount magnetic anomaly (southern Tyrrhenian Sea, Italy). *J Geophys Res* 114:B02103
- Carbotte SM, Smith DK, Cannat M, Klein EM (2015) Tectonic and magmatic segmentation of the Global Ocean Ridge System: a synthesis of observations. In: Wright TJ, Ayele A, Ferguson DJ, Kidane T, Vye-Brown C (eds) *Magmatic rifting and active volcanism*, vol 420. Geological Society London Special Publications, pp 1–47
- Carlson RL (2014) The influence of porosity and crack morphology on seismic velocity and permeability in the upper oceanic crust. *Geochem Geophys Geosyst* 15. <http://dx.doi.org/10.1002/2013GC004965>
- Chu D, Gordon R (1998) Current plate motions across the Red Sea. *Geophys J Int* 135:313–328
- Cochran JR (1983) A model for the development of the Red Sea. *Bull Am Assoc Petrol Geol* 67:41–69
- Cochran JR (2005) Northern Red Sea: nucleation of an oceanic spreading center within a continental rift. *Geochem Geophys Geosyst* 6:Q03006. <https://doi.org/10.1029/2004GC000826>
- Coleman RG (1973) Geological map of the Red Sea. U.S. Geological Survey, scale 1:2,000,000
- Coleman RG, McGuire AV (1988) Magma systems related to the Red-Sea opening. *Tectonophysics* 150:77–100
- Courtillot V (1982) Propagating rifts and continental breakup. *Tectonics* 1:239–250
- DeMets C, Gordon RG, Argus DF (2010) Geologically current plate motions. *Geophys J Int* 181:1–80
- Dick HJB, Lin J, Schouten H (2003) An ultraslow-spreading class of ocean ridge. *Nature* 426:405–412
- Drachev SS, Kaul N, Beliaev VN (2003) Eurasia spreading basin to Laptev Shelf transition: structural pattern and heat flow. *Geophys J R Astron Soc* 152:688–698
- Driesner T, Heinrich CA (2007) The system H₂O–NaCl. Part I: correlation formulae for phase relations in temperature–pressure–composition space from 0 to 1000 °C, 0 to 5000 bar, and 0 to 1 XNaCl. *Geochim Cosmochim Acta* 71:4880–4901
- Egloff F, Rihm R, Makris J, Izzeldin Y, Bobsien M, Meier K, Junge P, Noman T, Warsi W (1991) Contrasting structural styles of the eastern and western margins of the southern Red-Sea—the 1988 SONNE experiment. *Tectonophysics* 198:329–353
- Feldens P, Mitchell NC (2015) Salt flows in the central Red Sea. In: Rasul NMA, Stewart ICF (eds) *The Red Sea: the formation, morphology, oceanography and environment of a young ocean basin*. Springer Earth System Sciences, Berlin, pp 205–218
- Geshi N, Németh K, Oikawa T (2011) Growth of phreatomagmatic explosion craters: a model inferred from Suoana crater in Miyakejima Volcano, Japan. *J Volcanol Geotherm Res* 201:30–38
- Ghebreab W (1998) Tectonics of the Red Sea region reassessed. *Earth-Sci Rev* 45:1–44
- Gilbert LA, Salisbury MH (2011) Oceanic crustal velocities from laboratory and logging measurements of Integrated Ocean Drilling Program Hole 1256D. *Geochem Geophys Geosyst* 12:Q09001. <https://doi.org/10.1029/2011GC003750>
- Girdler RW (1985) Problems concerning the evolution of oceanic lithosphere in the northern Red Sea. *Tectonophysics* 116:109–122
- Girdler RW, Evans TR (1977) Red Sea heat flow. *Geophys J Int* 51:245–251
- Girdler RW, Styles P (1974) Two stage Red Sea floor spreading. *Nature* 247:7–11
- Girdler RW, Underwood M (1985) The evolution of early oceanic lithosphere in the southern Red Sea. *Tectonophysics* 116:95–108
- Girdler RW, Whitmarsh RB (1974) Miocene evaporites in Red Sea cores, their relevance to the problem of the width and age of oceanic crust beneath the Red Sea. *Init Rep Deep Sea Drill Proj* 2:913–921
- Grachev AF (2003) The Arctic rift system and the boundary between the Eurasian and North American lithospheric plates: new insight to plate tectonic theory. *Rus J Earth Sci* 5:307–345
- Guennoc P, Pautot G, Coutelle A (1988) Surficial structures of the northern Red Sea axial valley from 23°N to 28°N: time and space evolution of neo-oceanic structures. *Tectonophysics* 153:1–23

- Gurvich EG (2006) Metalliferous sediments of the Red Sea. *Metalliferous Sediments of the World Ocean*. Springer, Berlin, pp 127–210
- Haase KM, Muhe R, Stoffers P (2000) Magmatism during extension of the lithosphere: geochemical constraints from lavas of the Shaban Deep, northern Red Sea. *Chem Geol* 166:225–239
- Hewitt A, Salisbury R, Wilson J (2010) Using multibeam echosounder backscatter to characterize seafloor features. *Sea Technol* 51:10–13
- Izzeldin AY (1987) Seismic, gravity and magnetic surveys in the central part of the Red Sea; their interpretation and implications for the structure and evolution of the Red Sea. *Tectonophysics* 143:269–306
- Kerrick R, Polat A (2006) Archean greenstone-tonalite duality: thermochemical mantle convection models or plate tectonics in the early Earth global dynamics? *Tectonophysics* 415:141–165
- Levi S, Riddihough R (1986) Why are marine magnetic anomalies suppressed over sedimented spreading centers? *Geology* 14:651–654
- Ligi M, Bonatti E, Bortoluzzi G, Cipriani A, Cocchi L, Caratori Tontini F, Carminati E, Ottolini L, Schettino A (2012) Birth of an ocean in the Red Sea: initial pangs. *Geochem Geophys Geosyst*. <https://doi.org/10.1029/2012GC004155>
- Little SA, Stephen RA, Honnorez J, Adamson AC, Alt JC, Emmermann R, Becker K (1985) Costa Rica Rift borehole seismic experiment, Deep Sea Drilling Project Hole 504B, Leg 92. *Init Rep Deep Sea Drill Proj* 83:517–528
- Manheim FT, Waterman LS, Woo CC, Sayles FL (1974) Interstitial water studies on small core samples, Leg 23 (Red Sea). In: Supko PR, Weser OE (eds) *Initial reports of the deep sea drilling program*. U.S. Government Printing Office, Washington, pp 955–967
- Miller NC, Lizarralde D (2013) Thick evaporites and early rifting in the Guaymas Basin, Gulf of California. *Geology* 41:283–286
- Mitchell NC (1993) A model for attenuation of backscatter due to sediment accumulations and its application to determine sediment thicknesses with Gloria sidescan sonar. *J Geophys Res* 98:22477–22493
- Mitchell NC, Augustin N (2017) Halokinetics and other features of GLORIA long-range sidescan sonar data from the Red Sea. *Mar Pet Geol* 88:724–738
- Mitchell NC, Park Y (2014) Nature of crust in the central Red Sea. *Tectonophysics* 628:123–139
- Mitchell NC, Ligi M, Ferrante V, Bonatti E, Rutter E (2010) Submarine salt flows in the central Red Sea. *Bull Geol Soc Am* 122:701–713
- Mitchell NC, Ligi M, Feldens P, Hubscher C (2015) Deformation of a young salt giant: regional topography of the Red Sea Miocene evaporites. *Basin Res* 29(Suppl 1):352–369
- Moore DJG, Evans DBW (1967) The role of olivine in the crystallization of the prehistoric Makaopuhi tholeiitic lava lake, Hawaii. *Contrib Mineral Petrol* 15:202–223
- Pautot G, Guennoc P, Coutelle A, Lyberis N (1984) Discovery of a large brine deep in the northern Red Sea. *Nature* 310:133–136
- Prodehl C, Mechie J (1991) Crustal thinning in relationship to the evolution of the Afro-Arabian rift system—a review of seismic-refraction data. *Tectonophysics* 198:311–327
- Ross DA, Schlee J (1973) Shallow structure and geologic development of the southern Red Sea. *Bull Geol Soc Am* 84:3827–3848
- Sandwell DT, Mueller RD, Smith WHF, Garcia E, Francis R (2014) New global marine gravity model from CryoSat-2 and Jason-1 reveals buried tectonic structure. *Science* 346:65–67
- Sato H, Taniguchi H (1997) Relationship between crater size and ejecta volume of recent magmatic and phreato-magmatic eruptions: implications for energy partitioning. *Geophys Res Lett* 24:205–208
- Schettino A, Macchiavelli C, Pierantoni PP, Zanoni D, Rasul N (2016) Recent kinematics of the tectonic plates surrounding the Red Sea and Gulf of Aden. *Geophys J Int* 207:457–480
- Schmidt M, Devey CW, Eisenhauer A (2011) FS POSEIDON Cruise Report P408. *Berichte aus dem Leibniz-Institut fur Meereswissenschaften an der Christian-Albrechts-Universitat zu Kiel* 46
- Schmidt M, Al-Farawati R, Al-Aidaros A, Kurten B (2013) RV PELAGIA Cruise Report 64PE350/64PE351. *Berichte aus dem Helmholtz-Zentrum fur Ozeanforschung Kiel (GEOMAR)* 5
- Schofield N, Alsop I, Warren J, Underhill JR, Lehne R, Beer W, Lukas V (2014) Mobilizing salt: magma-salt interactions. *Geology* 42:599–602
- Searle RC, Ross DA (1975) A geophysical study of the Red Sea axial trough between 20.5° and 22°N. *Geophys J Int* 43:555–572
- Stoffers P, Kuhn R (1974) Red Sea evaporites: a petrographic and geochemical study. In: Supko PR, Weser OE (eds) *Initial reports of the deep sea drilling program*. U.S. Government Printing Office, Washington, pp 821–847
- Stoffers P, Ross DA (1974) Sedimentary history of the Red Sea. In: Supko PR, Weser OE (eds) *Initial reports of the deep sea drilling program*. U.S. Government Printing Office, Washington, pp 849–865
- Sultan M, Becker R, Arvidson RE, Shore P, Stern RJ, Elalfy Z, Guinness EA (1992) Nature of the Red-Sea crust—a controversy revisited. *Geology* 20:593–596
- Sultan M, Becker R, Arvidson RE, Shore P, Stern RJ, Elalfy Z, Attia RI (1993) New constraints on Red-Sea rifting from correlations of Arabian and Nubian Neoproterozoic outcrops. *Tectonics* 12:1303–1319
- Swift S, Reichow M, Tikku A, Tominaga M, Gilbert L (2008) Velocity structure of upper ocean crust at Ocean Drilling Program Site 1256. *Geochem Geophys Geosyst* 9, Q10O13. <http://dx.doi.org/10.1029/2008GC002188>
- Taylor B, Goodliffe AM, Martinez F, Hey R (1995) Continental rifting and initial sea-floor spreading in the Woodlark basin. *Nature* 374:534–537
- Taylor B, Goodliffe AM, Martinez F (1999) How continents break up: insights from Papua New Guinea. *J Geophys Res* 104:7497–7512
- Tramontini C, Davies D (1969) A seismic refraction survey in the Red Sea. *Geophys J Int* 17:225–241
- van der Zwan FM, Devey CW, Augustin N, Almeev RR, Bantan RA, Basaham A (2015) Hydrothermal activity at the ultraslow- to slow-spreading Red Sea Rift traced by chlorine in basalt. *Chem Geol* 405:63–81
- Walker GPL (1973) Explosive volcanic eruptions—a new classification scheme. *Geol Rundsch* 62:431–446
- White R, McKenzie D (1989) Magmatism at rift zones: the generation of volcanic continental margins. *J Geophys Res* 94(B6):7685–7729
- Whitmarsh RB, Manatschal G, Minshull TA (2001) Evolution of magma-poor continental margins from rifting to seafloor spreading. *Nature* 413:150–154